Progress In Electromagnetics Research, PIER 85, 195–210, 2008

IMAGE RECONSTRUCTION OF THE BURIED METALLIC CYLINDER USING FDTD METHOD AND SSGA

C.-H. Huang, C.-C. Chiu, C.-L. Li, and Y.-H. Li

Electrical Engineering Department
Tamkang University
Tamsui, Taiwan, R.O.C.

Abstract—This paper presents an image reconstruction approach based on the time-domain and steady state genetic algorithm (SSGA) for a 2-D perfectly conducting cylinder buried in a half-space. The computational method combines the finite difference time domain (FDTD) method and the steady state genetic algorithms (SSGA) to determine the shape and location of the subsurface scatterer with arbitrary cross section. The subgirdding technique is implemented in the FDTD code for modeling the shape of the cylinder more closely. In order to describe a a unknown 2-D cylinder with arbitrary cross section more effectively, the shape function is expanded by closed cubic-spline function instead of frequently used trigonometric series. The inverse problem is reformulated into an optimization problem and the global searching scheme SSGA with closed cubic-spline is then employed to search the parameter space. Numerical results show that the shadowing effect for the inverse problem in a half space results in poor image reconstruction on the backside of the cylinder. We propose the two-step strategy to overcome the shadowing effect. It is found that good imaging quality could be attained based on the proposed strategy.

1. INTRODUCTION

The objective of the inverse problem of the buried scatterer is to determine the electromagnetic properties of the scatterer from scattering field measured outside. Due to large domain of applications such as non-destructive problem, medical imaging, geophysical prospecting and determination of underground tunnels and pipelines, etc., the inverse scattering problems related to the buried bodies have a particular importance in the scattering theory. This kind of problem

is expected to be more difficult due to the fact that the information about the buried unknown scatterer obtained by the limited-view measurement is less than the full-view measurement. Although the incompleteness of the measurement data and the multiple scattering of the scatterer bring out the intrinsic non-unique and ill-posedness of these problems that appear consequentially in the inverse scattering problems [1, 2], the study can be applied in widespread use.

In the past ten years, the inversion techniques are developed intensively for the microwave imaging both in frequency domain and time domain [3–23]. Most of the inversion techniques are investigated for the inverse problem using only single frequency scattering data (monochromatic source) [3–10]. However, the time domain scattering data is important for the inverse problem because the available information content about scatterer is more than the only single frequency scattering data. Therefore, various time domain inversion approaches are proposed [11–17] that could be briefly classified as the neural networks [11], the layer-stripping approach [12], the iterative approach: Born iterative method (BIM) [13–15] and optimization approach [16, 17]. Traditional iterative inverse algorithms are founded on a functional minimization via some gradient-type scheme. In general, during the search of the global minimum, they tend to get trapped in local minima when the initial guess is far from the exact one. Genetic algorithm (GA) [18] is well-known evolutionary algorithm of optimization strategy, which uses stochastic mechanism to search through the parameter space. In recent year, most of the researchers have applied GA together with the frequency domain EM solver for the inverse problems [4–10]. Fewer researchers had applied the genetic/evolutionary algorithms in the time domain inverse scattering problem for metallic target identification [19, 20] and penetrable object reconstruction [21–23]. To the best of our knowledge, there is still no investigation on using the GA to reconstruct the electromagnetic imaging of metallic cylinders with arbitrary cross section in a half space under time domain.

This paper presents a time domain computational scheme for the microwave imaging of a 2-D metallic cylinder with arbitrary cross section buried in the subsurface. The forward problem is solved based on the FDTD method, for which the subgridding technique is implemented to closely describe the fine structure of the cylinder [24, 25]. Interpolation technique through the closed cubic B-splines [26] is employed to describe a 2-D cylinder with arbitrary cross section more effectively. The inverse problem is formulated into an optimization one and then the non-uniform steady state genetic algorithm (NU-SSGA) [8] previously published by the authors is used

to search the parameter space.

In Section 2, the subgridding FDTD method for the forward scattering are presented. In Section 3, the numerical results of the proposed inverse problem are given. The shadowing effect is shown, and the techniques proposed to overcome it are demonstrated. Finally, in Section 4 some conclusions are drawn for the proposed time domain inverse scattering.

2. FORWARD PROBLEM

Consider a 2-D metallic cylinder embedded in a half-space material medium as shown in Figure 1. The direct scattering problem is to calculate the scattered electric fields while the shape and location of the scatterer is given. The cylinder is assumed infinite long in z direction, while the cross-section shape is arbitrary in this study. The object is illuminated by Gaussian pulse line source located at the points denote by Tx in the first layer and only reflected waves are recorded at those points denoted by Rx in the same layer. The computational domain is discretized by the Yee's cell. It should be mentioned that the computational domain is surrounded by the optimized PML absorber [27] to reduce the reflection from the air-PML interface.

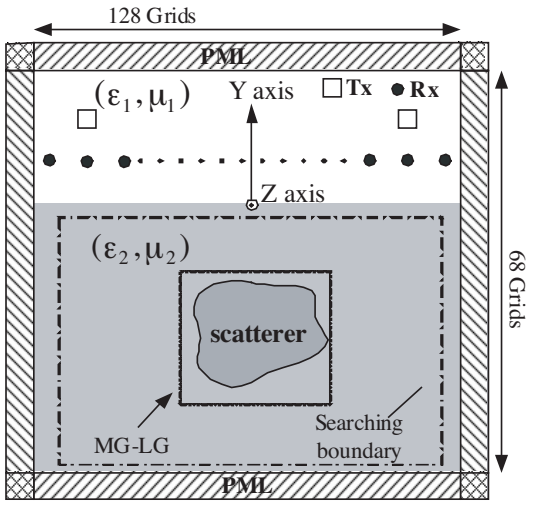

Figure 1. Geometrical configuration for the inverse scattering.

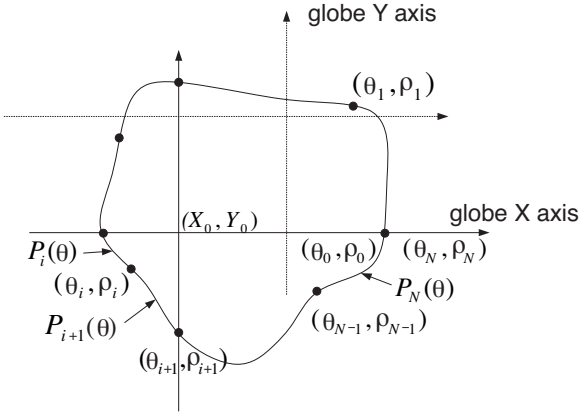

Figure 2. Geometry of the cubic-spline. (θ_i, ρ_i) is the polarized-coordinate expression for each point and $P_i(\theta)$ is the function of the cubic line which links the points $(\theta_{i-1}, \rho_{i-1})$ and (θ_i, ρ_i).

2.1. Cubic Spline Interpolation Technique

The local shape function $F(\theta)$ of the scatterer is approximated by the closed cubic B-splines for the sake of reducing the unknowns required to describe the arbitrary cross section more effectively. As shown in Figure 2, the boundary of the shape of the scatterer could be separated into N pieces which is consisted of the polynomials of degree 3 $P_i(\theta)$, $i = 1, 2, \cdots, N$ and have separated $N + 1$ points. The closed cubic spline, which satisfy the following smooth conditions:

$$\begin{aligned} &P_i(\theta_i) = P_{i+1}(\theta_i) = \rho_i \\ &P_i'(\theta_i) = P_{i+1}'(\theta_i) \qquad i = 1, 2, \cdots, N \\ &P_i''(\theta_i) = P_{i+1}''(\theta_i) \end{aligned} \tag{1}$$

and

$$\begin{aligned} &P_1(\theta_0) = P_N(\theta_N) \\ &P_1'(\theta_0) = P_N'(\theta_N) = \rho_N' \\ &P_N''(\theta_0) = P_N''(\theta_N) \end{aligned} \tag{2}$$

Through the interpolation of the cubic spline, an arbitrary smooth cylinder can be easily described through a few parameters $\rho_1, \rho_2, \ldots, \rho_N$ and the slope [26]. In order to closely describe the shape of the cylinder for the forward scattering procedure, the subgridding technique is implemented in the FDTD code, the details are presented as follows.

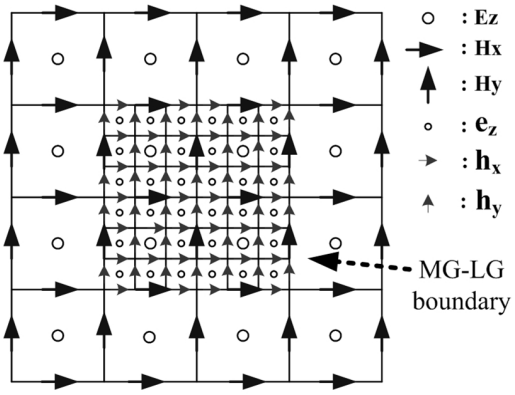

Figure 3. Structure of the TM_z FDTD major grids and local grids for the scaling ratio (1:3) : H fields are aligned with the MG-LG boundary.

2.2. Subgrid FDTD

A subgridding scheme is employed to divide the problem space into regions with different grid sizes. The grid size in coarse region is about $\left(\frac{1}{20} \sim \frac{1}{10}\lambda_{\max}\right)$ as in normal FDTD, while in the fine region the grid size is scaled by an integer ratio. As an example, the Yee cells with subgridding structure are shown in Figure 3, of which the scaling ratio is 1:3. The capital and small case letters stand for EM fields on the major grids and local grids, respectively. If the scaling ratio is set at odd-ratio then the fields are collocated in space at coarse and fine region. The e and h fields inside the fine region can be updated through the normal Yee-cell algorithm except those at the MG-LG boundary. The noncollocated magnetic field at the MG-LG interface can be obtained by linearly interpolation. The time interpolation of the fine grid magnetic field at the MG-LG interface is performed using the extra parabolic interpolation calculation.

For the time domain scattering and/or inverse scattering problem, the scatterers can be assigned with the fine region such that the fine structure can be easily described. If higher resolution is needed, only the fine region needs to be rescaled using a higher ratio for subgridding. This can avoid gridding the whole problem space using the finest resolution such that the computational resources are utilized in a more efficient way, which is quite important for the computational intensive inverse scattering problems.

3. INVERSE PROBLEM

For the inverse scattering problem, the shape, size and location of the metallic cylinder are reconstructed by the given scattered electric field obtained at the receivers. This problem is resolved by an optimization approach, for which the global searching scheme NU-SSGA previously reported by the author is employed to maximize the following fitness:

$$fit = \frac{1}{\sum_{n=1}^{N_i} \sum_{m=1}^{M} \sum_{t=0}^{T} \left| E_z^{\exp}(n,m,t) - E_z^{cal}(n,m,t) \right|} \tag{3}$$

where $E_z^{\exp}$ and E_z^{cal} are experimental electric fields and the calculated electric fields, respectively. The N_i and M are the total number of the transmitters and receivers, respectively. T is the time duration of the recorded electric fields.

The flowchart of the applied time domain inverse scattering algorithm is illustrated in Figure 4.

The genetic algorithms are very powerful stochastic global optimization methods based on genetic recombination and evaluation in nature [18]. GAs have been widely applied to the global numerical optimization problem in field of science and engineering. In general, a typical GA optimizer must be able to perform seven basic tasks:

1. Encode the solution parameters as genes,
2. Create a string of the genes to form a chromosome,
3. Initialize a starting population,
4. Evaluate and assign fitness values to individuals in the population,
5. Perform reproduction through some selection scheme,
6. Perform recombination of genes to produce offspring, and
7. Perform mutation of genes to produce offspring.

The key distinction between an NU-SSGA and a typical GA is on the number of fitness calculation. In a typical GA, each generation of the algorithm replaces the population with the new population. On the contrary, NU-SSGA only needs to generate a few offspring, by crossover and non-uniform beta distribution in mutation, to replace the weakest individual in each new generation. In other words, the number of fitness calculation corresponding to the new population is large in a typical GA compared with NU-SSGA. Based on the characteristic of NU-SSGA in reducing the numbers of fitness calculation, we are able to reconstruct the microwave image efficiently.

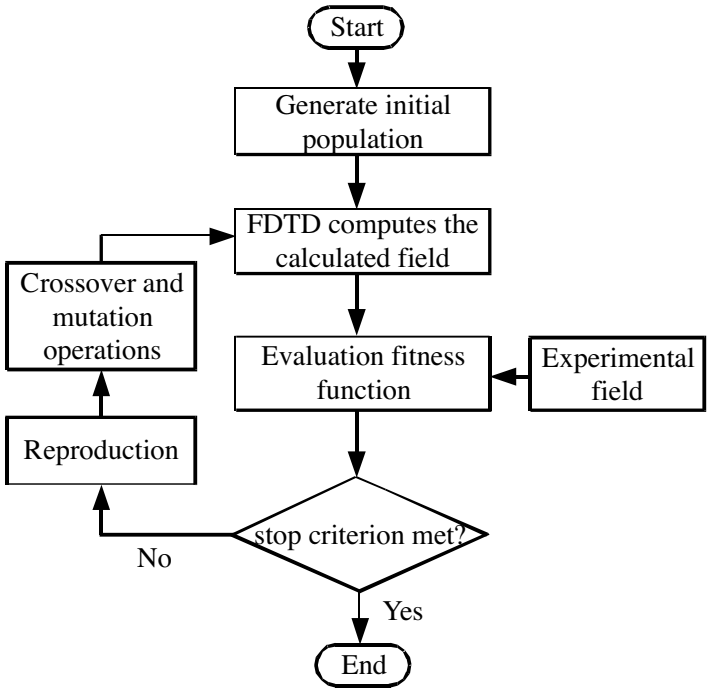

Figure 4. Flowchart for solving time domain inverse scattering problem.

4. NUMERICAL RESULTS

As shown in Figure 1, the problem space is divided in 128×68 grids with the grid size $\Delta x = \Delta y = 1.47\,\text{cm}$. The metallic cylinder is buried in lossless half space ($\sigma_1 = \sigma_2 = 0$). The transmitters and receivers are placed in free space above the homogeneous dielectric. The permittivities in region 1 and region 2 are characterized by $\varepsilon_1 = \varepsilon_0$ and $\varepsilon_2 = 2.3\varepsilon_0$, respectively, while the permeability μ_0 is used for each region, i.e., only non-magnetic media are concerned here. The cylindrical object is illuminated by a transmitter at two different positions, $N_i = 2$, which are located at the $(-61.74\,\text{cm},\ 22.05\,\text{cm})$ and $(61.74\,\text{cm},\ 22.05\,\text{cm})$, respectively. The scattered E fields for each illumination are collected at the fifteen receivers, $M = 15$, which are equally separated by 11.8 cm along the distance of 11.74 cm from the origin. The excitation waveform $E_z(t)$ of the transmitter is the

Gaussian pulse, given by:

$$E_z(t) = \begin{cases} Ae^{-\alpha(t-\beta\Delta t)^2}, & t \le T_w \\ 0, & t > T_w \end{cases} \tag{4}$$

where $\beta = 17$, $A = 1000$, $\Delta t = 34.685\,\text{ps}$, $T_w = 2\beta\Delta t$, and $\alpha = \left(\frac{1}{4\beta\Delta t}\right)^2$.

There are 400 samples of the scattering field for each illumination corresponding to the time duration of 13.874 ns. The cutoff frequency corresponding to the (4) is about 1.3 GHz. Note that in order to accurately describe the shape of the cylinder, the subgridding FDTD technique is used both in the forward scattering (1:9) and the inverse scattering (1:5) parts — but with different scaling ratios as indicated in the parentheses. For the forward scattering, the E fields generated by the FDTD with fine subgrids are used to mimic the experimental data in (3).

Three examples are investigated for the inverse scattering of the proposed structure by using the NU-SSGA algorithm. There are eleven unknown parameters to retrieve, which include the center position (X_o, Y_o), the radius ρ_i, $i = 1, 2, \ldots, 8$ of the shape function and the slope ρ'_N. Very wide searching ranges are used for the NU-SSGA to optimize the objective function given by (3). The parameters and the corresponding searching ranges are listed as follows: $-85.26\,\text{cm} \le X_o \le 85.26\,\text{cm}$, $-55.86\,\text{cm} \le Y_o \le 0\,\text{cm}$, $0\,\text{cm} \le \rho_i \le 11.8\,\text{cm}$, $i = 1, 2, \ldots, 8$ and $-1 \le \rho'_N \le 1$. The relative coefficients of the NU-SSGA are set as below: The crossover rate and the mutation rate are set to 0.1 and 0.05, respectively. The population size set 160 and the rank is set to 120.

The first example, a simple circular cylinder is tested, of which the shape function $F(\theta)$ is chosen to be $F(\theta) = 7.352\,\text{cm}$. The reconstructed shape of the best population member (chromosome) is plotted in Figure 5 for different generation. In Figure 4, it is observed that the front-side of the reconstructed image with respect to the incident waves is first achieved during the reconstructing procedure. Figure 5 also shows that even reconstructed cylinder position (X_0^c, Y_0^c) at 2000th generation is far away from exact one, the cubic spline interpolation technique can still recover it well. The r.m.s. error (DF) of the reconstructed shape $F^{cal}(\theta)$ with respect to the exact values

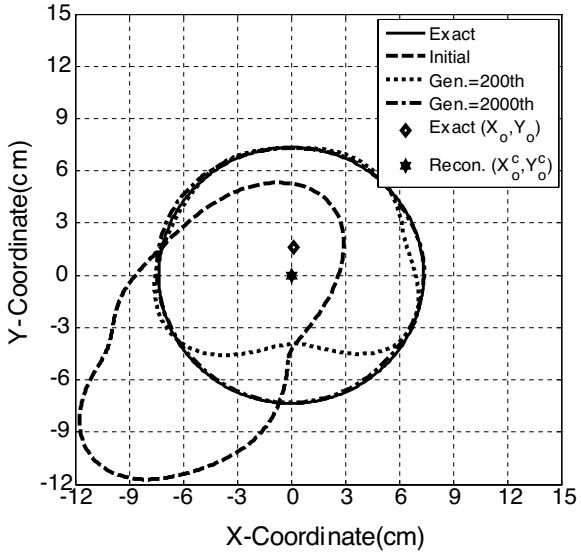

Figure 5. The reconstructed shape of the cylinder at different generations for example 1.

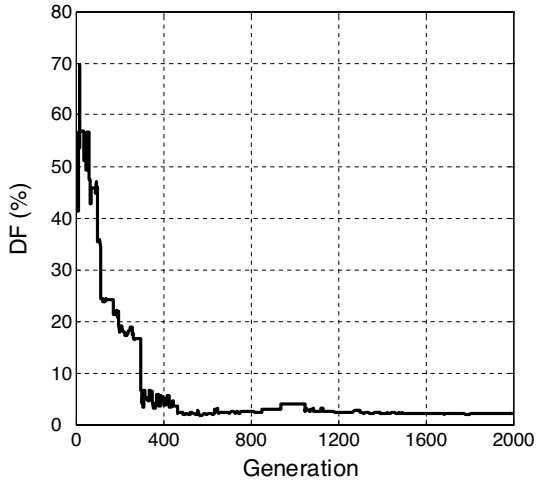

Figure 6. Shape function error at each generation of example 1.

versus generation are shown in Figure 6. Here, DF is defined as

$$DF = \left\{ \frac{1}{N'} \sum_{i=1}^{N'} \left[F^{cal}(\theta_i) - F(\theta_i) \right]^2 / F^2(\theta_i) \right\}^{1/2}, \quad \theta_i = \frac{2\pi}{N'} i \qquad (5)$$

where the N' is set to 1200. The r.m.s. error DF is about 2.3% in final. It is seen that the reconstruction is excellent.

In second example, the shape function of the unknown scatterer is selected by the cubic-spline expand to be $\rho_0 = 4.41\,\text{cm}$, $\rho_1 = 5.88\,\text{cm}$, $\rho_2 = 7.35\,\text{cm}$, $\rho_3 = 5.88\,\text{cm}$, $\rho_4 = 4.41\,\text{cm}$, $\rho_5 = 7.35\,\text{cm}$, $\rho_6 = 4.41\,\text{cm}$, $\rho_7 = 7.35\,\text{cm}$, and slope is 0. The reconstructed images for different generations are shown in Figure 7. The achieved shape error is about 16.07% at 2000th generation. It is observed that the shape on the backside of the cylinder is relatively poor due to the shadowing effect.

In order to improve the reconstructed quality, the two-step strategy is proposed to overcome the shadowing effect. The first step of the strategy is to illuminate the buried scatterer using the narrow Gaussian pulse (unipolar pulse) to obtain the rough dimension of the scatterer. The second step is to use the bipolar pulse called nearly resonant technique [20] (instead of unipolar Gaussian pulse). The main idea is to impress more energy around the transverse resonant frequency of the cylinder in order to gather more information of the cylinder structure. After the first step of the strategy, the perimeter of the reconstructed cylinder could be obtained by

$$L = \int_0^{2\pi} \sqrt{\left[F_{first}^{cal}(\theta)\right]^2 + \left[F'^{cal}_{first}(\theta)\right]^2}\, d\theta \tag{6}$$

The perimeter of the reconstructed cylinder in this example is about 39.85 cm. The transverse resonant frequency f_r is calculated by setting the perimeter of the cylinder equal to unit wavelength as follows:

$$f_r = \frac{c}{L\sqrt{\varepsilon_r}} = 496\,\text{MHz} \tag{7}$$

where L is the perimeter of the cylinder, ε_r the relative permittivity of the subsurface layer and c is the light velocity in free space. For the second step of the strategy, the nearly resonant bipolar pulse can now be determined by

$$E_z(t) = Ae^{-\alpha(t-\beta\Delta t)^2} \sin(2\pi f(t - \beta\Delta t)) \tag{8}$$

where $\beta = 48$, $f = \frac{1}{2\beta\Delta t}$ and the other parameters are the same as (4). The peak spectrum of exciting bipolar pulse is about 480 MHz which is quite close to 496 MHz.

The bipolar line source with the nearly resonant technique and the NU-SSGA is now tested for this example, while the all parameters unchanged. The reconstructed shapes by the nearly resonant technique

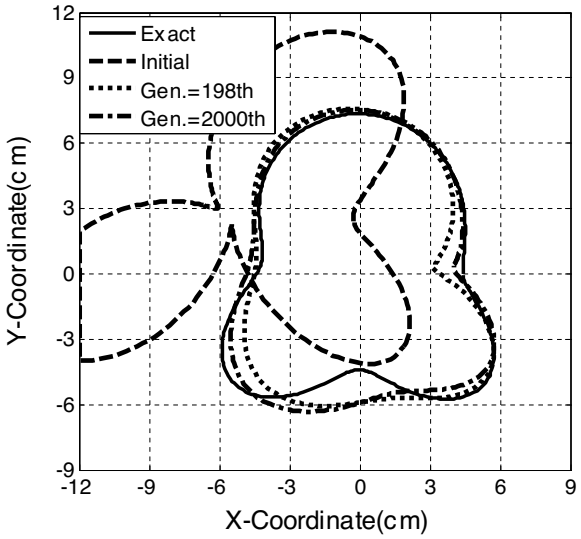

Figure 7. Reconstructed cross section of the cylinder for example 2 using the Gaussian pulse illumination.

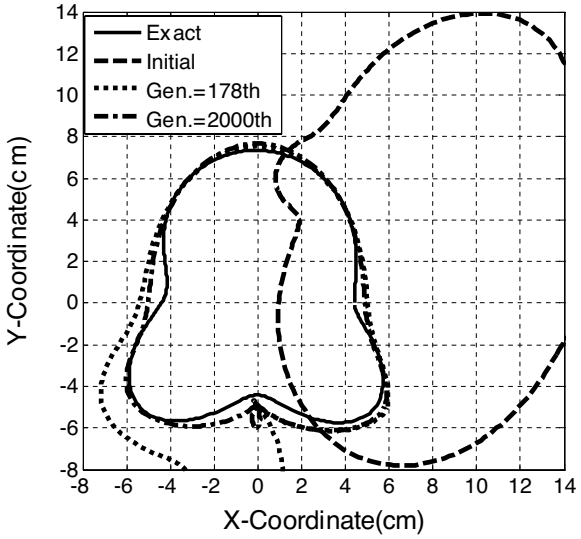

Figure 8. Reconstructed cross section of the cylinder for example 2 by two step strategy.

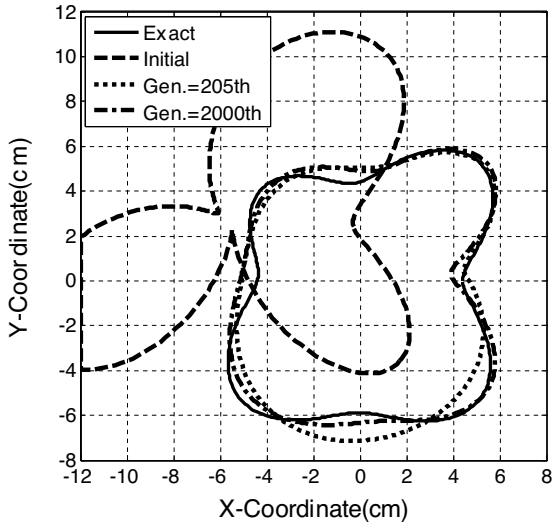

Figure 9. Reconstructed cross section of the cylinder for final example using the Gaussian pulse illumination.

at different generations are shown in Figure 8. The concave part of reconstructed shape at the 2000th generation is closer to the exact one as compared to Figure 7 of the unipolar Gaussian pulse case. The shape error is reduced from 16.07% to 12.32% for this case.

In final example, we consider the scatterer with $\rho_0 = 4.41$ cm, $\rho_1 = 7.35$ cm, $\rho_2 = 4.41$ cm, $\rho_3 = 5.88$ cm, $\rho_4 = 4.41$ cm, $\rho_5 = 7.35$ cm, $\rho_6 = 5.88$ cm and $\rho_7 = 7.35$ cm to test the effect of the two step strategy. The reconstructed images by only Gaussian line source illumination at different generations are shown in Figure 9. The achieved shape error is about 11.74% at 2000th generation. Figure 10 shows the reconstructed images by the two-step strategy, of which shape error is about 4.75% at 2000th generation. From the reconstructed results of these cases, we conclude the proposed two-step strategy can improve the reconstructed quality successfully to reduce the shadowing effect.

In order to investigate the sensitivity of the imaging algorithm against random noise, the additive white Gaussian noise of zero mean is added into the experimental electric fields. Normalize standard deviations of -30 dB, -20 dB, -10 dB, -5 dB and -3 dB are used in simulation purpose. The normalized standard deviation mentioned earlier is defined as the standard deviation of the Gaussian noise divided by the rms value of the scattered fields. Here, the signal-to-noise ratio (SNR) is inversely proportional to the normalized standard

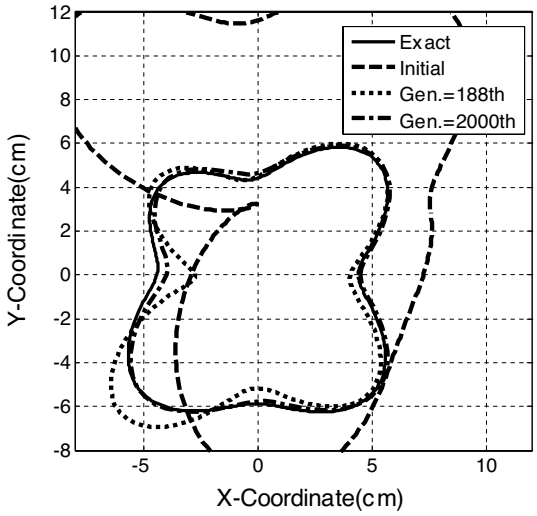

Figure 10. Reconstructed cross section of the cylinder of final example by two step strategy.

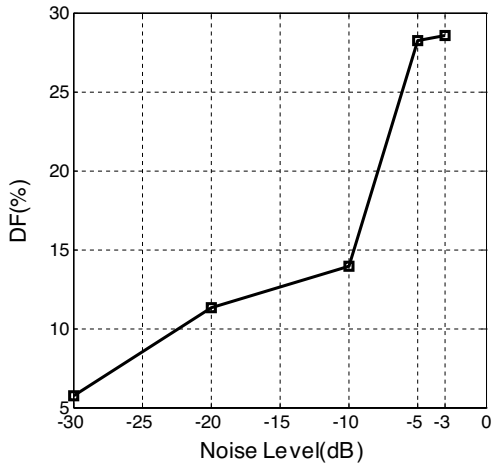

Figure 11. Shape error as functions of noise for final example.

deviation. Figure 11 shows the reconstructed results under the condition that the experimental scattered field is contaminated by noise. It could be observed that good reconstruction has been obtained for the shape of the buried metallic cylinder when the normalize standard deviations is above -10 dB.

5. CONCLUSION

In this paper, we study the time domain inverse scattering of an arbitrary cross section metallic cylinder buried in half space. By combining the FDTD method and the NU-SSGA, good reconstructed results are obtained. The subgridding scheme is employed to closely describe the shape of the cylinder for the FDTD method. In order to describe the shape of the scatterer more effectively cubic spline interpolation technique is utilized. The inverse problem is reformulated into an optimization one, and then the global searching scheme NU-SSGA is employed to search the parameter space. Some examples show the imaging quality of the backside of the scatterer is poor due to the shadowing effect. A novel two-step strategy is proposed to overcome the shadowing effect of inverse problem of the unreachable region, such as half space. By using the NU-SSGA, the shape and location of the object can be successfully reconstructed. In our study, even when the initial guess is far from the exact one the NU-SSGA can still yield a good solution for the properties of the object, while the gradient-based methods often get stuck in a local extreme. Numerical results have been carried out and good reconstruction has been obtained even in the presence of white Gaussian noise in experimental data.

REFERENCES

1. Kirsch, A. and R. Kress, "Uniqueness in inverse obstacle scattering," *Inverse Problems*, Vol. 9, 285–299, 1993.
2. Colton, D. and R. Kress, *Inverse Acoustic and Electromagnetic Scattering Theory*, Springer-Verlag, New York, 1992.
3. Ma, J., W. C. Chew, C. C. Lu, and J. Song, "Image reconstruction from TE scattering data using equation of strong permittivity fluctuation," *IEEE Transactions on Antennas and Propagation*, Vol. 48, No. 6, 860–867, June 2000.
4. Chien, W. and C. C. Chiu, "Using NU-SSGA to reduce the searching time in inverse problem of a buried metallic object," *IEEE Transactions on Antennas and Propagation*, Vol. 53, No. 10, 3128–3134, October 2005.
5. Qing, A., "An experimental study on electromagnetic inverse scattering of a perfectly conducting cylinder by using the real-coded genetic algorithm," *Microwave and Optical Technology Letters*, Vol. 30, 315–320, September 2001.
6. Caorsi, S., A. Massa, and M. Pastorino, "A computational technique based on a real-coded genetic algorithm for microwave

imaging purposes," *IEEE Transactions on Geoscience and Remote Sensing*, Vol. 38, No. 4, 1697–1708, July 2000.

7. Takenaka, T., Z. Q. Meng, T. Tanaka, and W. C. Chew, "Local shape function combined with genetic algorithm applied to inverse scattering for strips," *Microwave and Optical Technology Letters*, Vol. 16, 337–341, December 1997.
8. Li, C.-L., S.-H. Chen, C.-M. Yang, and C.-C. Chiu, "Image reconstruction for a partially immersed perfectly conducting cylinder using the steady state genetic algorithm," *Radio Sci.*, Vol. 39, RS2016, doi:10.1029/2002RS002742, 2004.
9. Huang, C.-H., Y.-F. Chen, and C.-C. Chiu, "Permittivity distribution reconstruction of dielectric objects by a cascaded method," *Journal of Electromagnetic Waves and Applications*, Vol. 21, No. 2, 145–159, 2007.
10. Wei, C., "Inverse scattering of an un-uniform conductivity scatterer buried in a three-layer structure," *Progress In Electromagnetics Research*, PIER 82, 1–18, 2008.
11. Bermani, E., S. Caorsi, and M. Raffetto, "Geometric and dielectric characterization of buried cylinders by using simple time-domain electromagnetic data and neural networks," *Microwave and Optical Technology Letters*, Vol. 24, No. 1, 24–31, January 2000.
12. Popovic, M. and A. Taflove, "Two-dimensional FDTD inverse-scattering scheme for determination of near surface material properties," *IEEE Transactions on Antennas and Propagation*, Vol. 52, No. 9, 2366–2373, September 2004.
13. Yu, W., Z. Peng, and L. Jen, "The time-domain Born iterative method for two-dimensional inhomogeneous lossy dielectric," *Journal of Microwaves*, Vol. 11, No. 12, 1995.
14. Moghaddam, M. and W. C. Chew, "Nonlinear two-dimensional velocity profile inversion using time-domain data," *IEEE Transactions on Geoscience and Remote Sensing*, Vol. 30, No. 1, 147–156, 1992.
15. Moghaddam, M. and W. C. Chew, "Study of some practical issues in inversion with the Born iterative method using time-domain data," *IEEE Transactions on Antennas and Propagation*, Vol. 41, No. 2, 177–184, 1993.
16. Rekanos, I. T., "Time-domain inverse scattering using lagrange multipliers: An iterative FDTD-based optimization technique," *Journal of Electromagnetic Waves and Applications*, Vol. 17, No. 2, 271–289, 2003.
17. Takenaka, T., H. Jia, and T. Tanaka, "Microwave imaging

of electrical property distributions by a forward-backward time-stepping method," *Journal of Electromagnetic Waves and Applications*, Vol. 14, 1609–1625, 2000.

18. Goldgerg, D. E., *Genetic Algorithm in Search, Optimization and Machine Learning*, Addison-Wesley, 1989.
19. Zhong, X.-M., C. Liao, and W. Chen, "Image reconstruction of arbitrary cross section conducting cylinder using UWB pulse," *Journal of Electromagnetic Waves and Applications*, Vol. 21, No. 1, 25–34, 2007.
20. Huang, C. H., S. H. Chen, C. L. Li, and C. C. Chiu, "Time domain inverse scattering of an embedded cylinder with arbitrary shape using nearly resonant technique," *2004 International Conference on Electromagnetic Applications and Compatibility*, Taipei, Taiwan, October 2004.
21. Chen, X. and K. Huang, "Microwave Imaging of buried inhomogeneous objects using parallel genetic algorithm combined with FDTD method," *Progress In Electromagnetics Research*, PIER 53, 283–298, 2005.
22. Choi, H.-K., S.-K. Park, and J.-W. Ra, "Reconstruction of a high-contrast penetrable object in pulsed time domain by using the genetic algorithm," *IEEE International Sym. on Geoscience and Remote Sensing*, Vol. 1, 136–138, 1997.
23. Chen, X., D. Liang, and K. Huang, "Microwave imaging 3-D buried objects using Parallel genetic algorithm combined with FDTD technique," *Journal of Electromagnetic Waves Application*, Vol. 20, No. 13, 1761–1774, 2006.
24. Chevalier, M. W., R. J. Luebbers, and V. P. Cable, "FDTD local grid with material traverse," *IEEE Trans. Antennas and Propagation*, Vol. 45, No. 3, March 1997.
25. Huang, C.-H., C.-C. Chiu, C.-L. Li, and K.-C. Chen, "Time domain inverse scattering of a two-dimensional homogenous dielectric object with arbitrary shape by particle swarm optimization," *Progress In Electromagnetics Research*, PIER 82, 381–400, 2008.
26. De Boor, C., *A Practical Guide to Splines*, Springer-Verlag, New York, 1978.
27. Li, C.-L., C.-W. Liu, and S.-H. Chen, "Optimization of a PML absorber's conductivity profile using FDTD," *Microwave and Optical Technology Lett.*, Vol. 37, 380–383, 2003.